

# Signs of superparamagnetic cluster formation in $\text{LuFe}_{1-x}\text{Cr}_x\text{O}_3$ perovskites evidenced by magnetization reversal and Monte Carlo simulations


Florencia E. Lurgo,<sup>1</sup> Orlando V. Billoni<sup>2,\*</sup>, Vladimir Pomjakushin,<sup>3</sup> Juan Pablo Bolletta<sup>4</sup>, Christine Martin,<sup>4</sup> Antoine Maignan<sup>4</sup>, and Raúl E. Carbonio<sup>1</sup>

<sup>1</sup>INFIQC (CONICET-UNC), Departamento de Físicoquímica, Facultad de Ciencias Químicas, Universidad Nacional de Córdoba, Haya de la Torre Esq. Medina Allende, Ciudad Universitaria, X5000HUA Córdoba, Argentina

<sup>2</sup>Facultad de Matemática, Astronomía, Física y Computación, Universidad Nacional de Córdoba and Instituto de Física Enrique Gaviola (IFEG-CONICET), Ciudad Universitaria, X5000HUA Córdoba, Argentina

<sup>3</sup>Laboratory for Neutron Scattering and Imaging (LNS), Paul Scherrer Institute, Villigen CH-5232, Switzerland

<sup>4</sup>Laboratoire CRISMAT, Normandie Univ, ENSICAEN, UNICAEN, CNRS, 14050 Caen, France

 (Received 6 July 2020; revised 28 December 2020; accepted 13 January 2021; published 29 January 2021)

In this paper, we study the magnetic properties of orthorhombic ( $Pbnm$ ) perovskites  $\text{LuFe}_{1-x}\text{Cr}_x\text{O}_3$  with  $x = 0.25, 0.45, 0.55$ , and  $0.75$  by magnetization vs temperature and neutron powder diffraction measurements at room temperature. The magnetic moments are oriented along the  $x$  direction with a  $\mathbf{G}$ -type antiferromagnetic (AFM) arrangement that corresponds to irreducible representation  $\Gamma_4$  ( $G_x A_y F_z$ ). Magnetization reversal (MR) is observed for  $0.45 \leq x \leq 0.75$ . The MR phenomenon was modeled using Monte Carlo simulations, modeling both homogeneous and inhomogeneous cation distributions. For  $\text{LuFe}_{0.25}\text{Cr}_{0.75}\text{O}_3$ , the presence of MR could only be explained using an inhomogeneous distribution with well-defined magnetic clusters. Looking at the staggered magnetization of each cluster, we propose a superparamagnetic regime of  $\text{Fe}^{3+}$  clusters in a  $\text{Cr}^{3+}$ -rich matrix for  $\text{LuFe}_{0.25}\text{Cr}_{0.75}\text{O}_3$ . By calculating the specific heat, we found that, in  $\text{LuFe}_{0.45}\text{Cr}_{0.55}\text{O}_3$  and  $\text{LuFe}_{0.25}\text{Cr}_{0.75}\text{O}_3$  the clusters order at nearly the same temperature  $T_N^{\text{clus}} \sim 535$  and  $520$  K, respectively, while the matrix orders at  $T_N^{\text{Mat}} \sim 115$  K. There is considerable reduction in the cluster ordering temperature as compared with the bulk, as  $T_N \sim 628$  K for  $\text{LuFeO}_3$ , while the matrix orders at the expected temperature as  $T_N \sim 115$  K for  $\text{LuCrO}_3$ .

DOI: [10.1103/PhysRevB.103.014447](https://doi.org/10.1103/PhysRevB.103.014447)

## I. INTRODUCTION

$\text{RMO}_3$  perovskites belong to a series of materials called orthochromites ( $M = \text{Cr}$ ) or orthoferrites ( $M = \text{Fe}$ ). It is a very well-known class of compounds which crystalizes in the  $Pbnm$  space group. Their structure consists of  $\text{MO}_6$  octahedra which share corners in all three directions (see Fig. S1 in the Supplemental Material [1]). The  $\text{R}^{3+}$  cations occupy every hole (Wyckoff site  $4c$ ) that is formed by eight  $\text{MO}_6$  octahedra, (with  $\text{M}^{3+}$  in the  $4b$  site) giving the  $\text{R}^{3+}$  cation a 12-fold oxygen coordination in the ideal case (when there are small tilts of the octahedra). The octahedra are tilted in the three directions. In  $a$  and  $b$  (of the pseudocubic cell), the tilt is in antiphase (Fig. S1a in the Supplemental Material [1]), and in phase in the  $c$  direction (Fig. S1b in the Supplemental Material [1]), giving rise to the Glazer's notation  $a^-a^-c^+$  [2]. These perovskites order antiferromagnetically (AFM) at a  $T_N$  depending on the transition metal. A weak ferromagnetic (WFM) component, which is caused by the canting of the magnetic moments in this AFM ordering, points along the  $c$  axis, presenting a  $\Gamma_4(G_x, F_z)$  magnetic structure at room temperature (RT).

Perovskites  $\text{RFe}_{1-x}\text{M}_x\text{O}_3$  ( $R =$  rare earth or Y, and  $M =$  Cr, Mn, or Co) have been studied in the last decades due to their interesting physical properties associated with the magnetic interactions between cations containing unpaired  $3d$  and/or  $4f$  electrons [3–8]. These interactions can produce a variety of behaviors, including spin reorientation [7,9–11], negative thermal expansion [6], multiferroicity [12–14], and magnetization reversal (MR) phenomena [6,14–16]. The latter is especially important for the development of new magnetocaloric materials and spintronic devices; it manifests as magnetization becoming opposite to an applied magnetic field. This happens due to the compensation of one magnetic sublattice with respect to another at a compensation temperature ( $T_{\text{comp}}$ ), below which the magnetization crosses zero and becomes negative [17]. MR has been observed in perovskites  $\text{RFe}_{1-x}\text{Cr}_x\text{O}_3$  [6]. Particularly when  $R$  is a nonmagnetic rare-earth cation such as  $\text{Lu}^{3+}$ ,  $\text{La}^{3+}$ , or  $\text{Y}^{3+}$  [17–20], MR is not superimposed to spin reorientation, and thus, its study is much simpler. These perovskites exhibit a WFM behavior below the ordering temperature ( $T_N$ ) due to a slight canting of the AFM ordered magnetic moments. WFM behavior can arise due to two different magnetic interactions: antisymmetric exchange or Dzyaloshinskii-Moriya (DM) interaction and single-ion magnetocrystalline anisotropy [21,22]. In perovskites with mixed occupation of the  $B$  site, such as  $\text{LuFe}_{0.5}\text{Cr}_{0.5}\text{O}_3$  and  $\text{YFe}_{0.5}\text{Cr}_{0.5}\text{O}_3$ , the

\*billoni@famaf.unc.edu.ar

TABLE I. Unit cell parameters, atomic positions, occupancies, displacement factors, reliability factors, and refined composition obtained from NPD at room temperature for  $\text{LuFe}_{0.75}\text{Cr}_{0.25}\text{O}_3$ ,  $\text{LuFe}_{0.55}\text{Cr}_{0.45}\text{O}_3$ ,  $\text{LuFe}_{0.45}\text{Cr}_{0.55}\text{O}_3$ , and  $\text{LuFe}_{0.25}\text{Cr}_{0.75}\text{O}_3$  perovskites.

Perovskite	$\text{LuFe}_{0.75}\text{Cr}_{0.25}\text{O}_3$	$\text{LuFe}_{0.55}\text{Cr}_{0.45}\text{O}_3$	$\text{LuFe}_{0.45}\text{Cr}_{0.55}\text{O}_3$	$\text{LuFe}_{0.25}\text{Cr}_{0.75}\text{O}_3$
$a$ (Å)	5.20714 (3)	5.20044 (3)	5.19604 (3)	5.18797 (3)
$b$ (Å)	5.54416 (4)	5.53265 (3)	5.52575 (4)	5.51481 (3)
$c$ (Å)	7.54321 (5)	7.52650 (4)	7.51690 (5)	7.49976 (4)
$V$ (Å <sup>3</sup> )	217.767 (2)	216.554 (2)	215.826 (2)	214.584 (9)
$R$ 4 $c$ ( $x, y, 1/4$ )				
$x$	0.98013 (2)	0.98037 (2)	0.98050 (1)	0.98032 (1)
$y$	0.07106 (1)	0.07055 (1)	0.07058 (1)	0.07025 (1)
$B$ (Å <sup>2</sup> )	0.401 (2)	0.490 (3)	0.506 (3)	0.388 (3)
(Fe,Cr) 4 $b$ (0,1/2,0)				
$B$ (Å <sup>2</sup> )	0.022 (2)	0.168 (2)	0.199 (2)	0.038 (1)
Occupancy	0.712 (2)/0.290 (2)	0.524 (1)/0.480 (1)	0.432 (2)/0.572 (2)	0.249 (2)/0.751 (2)
$\text{O}_1$ 4 $c$ ( $x, y, 1/4$ )				
$x$	0.11882 (2)	0.11804 (2)	0.11761 (2)	0.11660 (1)
$y$	0.45438 (2)	0.45588 (2)	0.45598 (2)	0.45700 (2)
$B$ (Å <sup>2</sup> )	0.091 (3)	0.352 (2)	0.335 (1)	0.076 (2)
$\text{O}_2$ 8 $d$ ( $x, y, z$ )				
$x$	0.68907 (1)	0.68934 (1)	0.68919 (1)	0.68950 (1)
$y$	0.30639 (1)	0.30615 (1)	0.30599 (1)	0.30550 (1)
$z$	0.06056 (1)	0.05962 (1)	0.05946 (1)	0.05880 (1)
$B$ (Å <sup>2</sup> )	0.312 (3)	0.435 (3)	0.473 (2)	0.363 (3)
Reliability factors				
$\chi^2$	1.62	1.27	1.33	1.22
$R_p$ (%)	7.46	7.44	7.4	7.6
$R_{wp}$ (%)	8.46	8.18	8.25	8.27
$R_{exp}$ (%)	6.64	7.26	7.16	7.49
$R_{Bragg}$ (%)	2.36	1.34	1.56	1.88
$R_{mag}$ (%)	3.32	5.54	8.12	5.26
Refined composition	$\text{LuFe}_{0.71}\text{Cr}_{0.29}\text{O}_3$	$\text{LuFe}_{0.52}\text{Cr}_{0.48}\text{O}_3$	$\text{LuFe}_{0.43}\text{Cr}_{0.57}\text{O}_3$	$\text{LuFe}_{0.25}\text{Cr}_{0.75}\text{O}_3$

WFM behavior is mainly related to the competition between superexchange interactions  $\text{Fe}^{3+}\text{-O}^{2-}\text{-Fe}^{3+}$ ,  $\text{Cr}^{3+}\text{-O}^{2-}\text{-Cr}^{3+}$  and  $\text{Fe}^{3+}\text{-O}^{2-}\text{-Cr}^{3+}$ , and DM interactions can be properly modeled using Monte Carlo (MC) simulations in a Heisenberg classical spin Hamiltonian [23–26]. Indeed, MC results show that, below  $T_N$ , the WFM component due to  $\text{Fe}^{3+}$  cations aligns in the direction of the applied magnetic field, while those of  $\text{Cr}^{3+}$  ions are aligned opposite to the magnetic field. The balance between these two net magnetizations is what gives rise to MR in these perovskites [23]. These ideas were used recently by Fita *et al.* [27] to explain experimental results of MR and exchange bias (EB) effects in  $\text{LuFe}_{0.5}\text{Cr}_{0.5}\text{O}_3$ . This paper showed that, in polycrystalline  $\text{LuFe}_{0.5}\text{Cr}_{0.5}\text{O}_3$  samples, MR is intrinsically associated with the EB phenomena. Particularly, EB arises in the coupling with the cooling field of short-range ordered regions rich in iron at temperatures above the Néel temperature; this coupling induces both positive and negative EB fields. These iron-rich zones are not expected in homogeneous samples with a high content of Cr, such as  $\text{LuFe}_{0.25}\text{Cr}_{0.75}\text{O}_3$ . Moreover, MC simulations in homogeneous systems indicate that, in  $\text{RFe}_{1-x}\text{Cr}_x\text{O}_3$  ( $R = \text{Lu}$  or  $\text{Y}$ ), MR can be explained at  $x = 0.4$  and departs from experiments at  $x = 0.5$  [6,23,28].

For these reasons, we have synthesized  $\text{LuFe}_{1-x}\text{Cr}_x\text{O}_3$  perovskites for  $x = 0.25, 0.45, 0.55$ , and  $0.75$  and studied their magnetic properties by a combination of magnetization

measurements, neutron powder diffraction (NPD), and MC simulations.

## II. EXPERIMENTAL

$\text{LuFe}_{1-x}\text{Cr}_x\text{O}_3$  with  $x = 0.25, 0.45, 0.55$ , and  $0.75$  compounds was prepared in powder form by a wet chemical method. Stoichiometric amounts of  $\text{Lu}_2\text{O}_3$ ,  $\text{Fe}(\text{NO}_3)_3 \cdot 9\text{H}_2\text{O}$ , and  $\text{Cr}(\text{NO}_3)_3 \cdot 9\text{H}_2\text{O}$  (99.9% Strem Chemicals) were dissolved in aqueous solution with 10 mL of concentrated  $\text{HNO}_3$  to facilitate the dissolution of  $\text{Lu}_2\text{O}_3$ . Once all the precursors have been dissolved, a 25% w/w citric acid solution was added. The citrate solution was slowly evaporated, leading to an organic resin that contained a homogeneous distribution of the cations. This resin was dried at 120 °C for 6 h and then decomposed at 600 °C for 12 h in air, with the aim of eliminating all organic matter. This treatment produced homogeneous and very reactive precursors that were finally heated at 1100 °C in air for 12 h with 5 °C/min warming and cooling rates. For  $\text{LuFe}_{0.25}\text{Cr}_{0.75}\text{O}_3$ , the powder was also crushed again, and two additional heat treatments were performed at 1250 and 1350 °C in air for 12 h with 5 °C/min warming and cooling rates. Above 1350 °C, these perovskites were found to melt.

X-ray powder diffraction (XRPD) patterns were collected at RT with a PANalytical X'Pert Pro diffractometer in Bragg-Brentano geometry with  $\text{Cu-K}\alpha$  radiation, in the  $2\theta$  angular

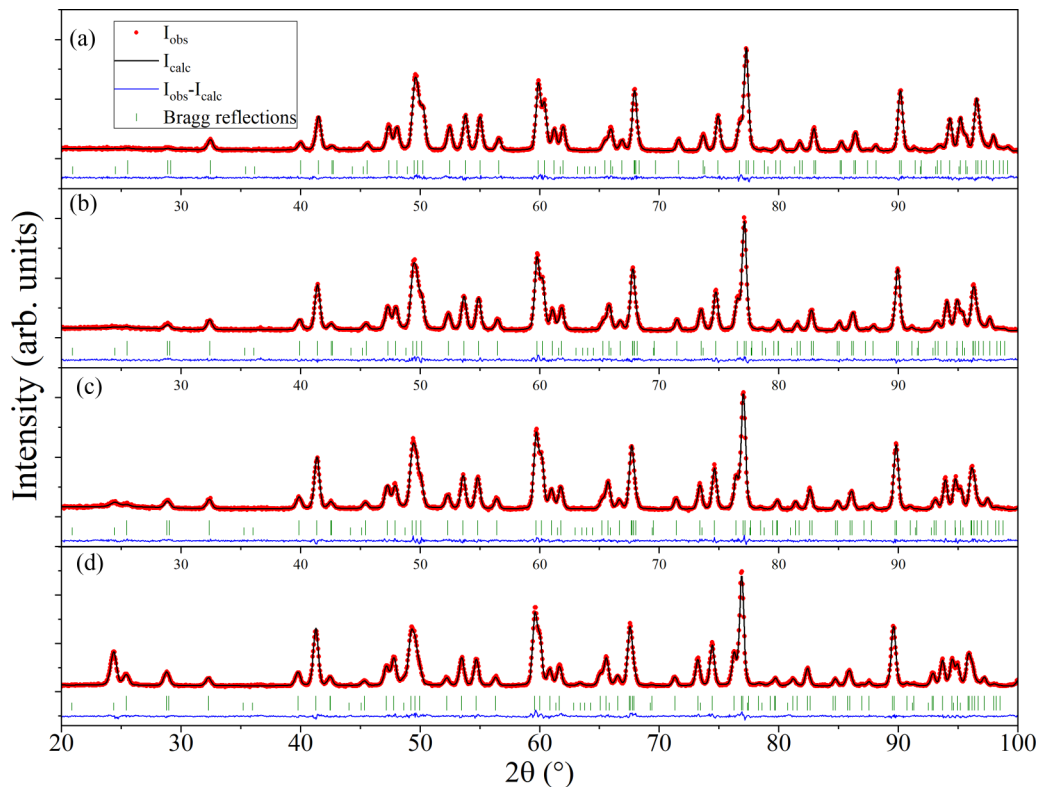


FIG. 1. Observed and calculated neutron powder diffraction (NPD) patterns at room temperature (RT) for: (a)  $\text{LuFe}_{0.25}\text{Cr}_{0.75}\text{O}_3$ , (b)  $\text{LuFe}_{0.45}\text{Cr}_{0.55}\text{O}_3$ , (c)  $\text{LuFe}_{0.55}\text{Cr}_{0.45}\text{O}_3$ , and (d)  $\text{LuFe}_{0.75}\text{Cr}_{0.25}\text{O}_3$ . Red circles: Experimental patterns. Continuous black line: Calculated patterns. Blue line: Difference. First set of green vertical lines: Reflections from nuclear structures. Second set of green vertical lines: Reflections from magnetic structures. Note that magnetic reflections (at low angles) are more intense as the amount of Fe increases. The whole NPD patterns, up to  $160^\circ$  in  $2\theta$  are shown in the Supplemental Material [1] (Fig. S2).

range of  $10\text{--}120^\circ$  in steps of  $0.02^\circ$  and with a collecting time of 10 s/step. NPD patterns were obtained in the HRPT instrument at the SINQ facility in the Paul Scherrer Institut (PSI). Patterns were collected at RT for each sample with  $\lambda = 1.8860 \text{ \AA}$  in the  $3.55^\circ$  to  $164.5^\circ$   $2\theta$  range with a  $0.05^\circ$  step. The refinement of crystal and magnetic structures was performed by using the Rietveld method [29] with the FULLPROF program [30].

Magnetic measurements were performed using a commercial MPMS-5S superconducting quantum interference device magnetometer on powder samples, warming from 5 to 400 K at 100 Oe in zero-field-cooled and field cooled (ZFC-FC) modes. Isothermal magnetization loops were performed from  $-5$  to  $+5$  T at 5 K for all samples.

### III. EXPERIMENTAL RESULTS

#### A. NPD and XRPD

XRPD was performed in all the samples, and the patterns were correctly refined with the  $Pbnm$  space group. Cell parameters as a function of composition are shown in Table S1 in the Supplemental Material [1]. The refinement using XRPD data of the samples treated at different temperatures does not evidence significant changes in the cell parameters.

These results are confirmed by the NPD data, which also allowed us to determine the actual ratio of  $\text{Fe}^{3+}/\text{Cr}^{3+}$ , due to the high difference in the scattering lengths: Fe (9.45

fm) and Cr (3.64 fm).  $\text{Lu}^{3+}$  and  $\text{O}^{2-}$  occupancies were also refined, but they remained constant within the third decimal figure, so they were fixed to their stoichiometric values. Table I summarizes the unit cell, atomic positions, occupancies, atomic displacement parameters, and reliability factors obtained from NPD data at RT. Additionally, the table also shows the refined chemical formulas obtained from the occupancy factors, which are in excellent agreement with the nominal compositions. Figure 1 shows the refined NPD patterns for  $\text{LuFe}_{0.25}\text{Cr}_{0.75}\text{O}_3$ ,  $\text{LuFe}_{0.45}\text{Cr}_{0.55}\text{O}_3$ ,  $\text{LuFe}_{0.55}\text{Cr}_{0.45}\text{O}_3$ , and  $\text{LuFe}_{0.75}\text{Cr}_{0.25}\text{O}_3$  at RT. Already at RT, a magnetic contribution to the NPD is observed at low angles, being more important as the Fe content increases. The corresponding refined magnetic moments are shown in Table II. A  $G_x$  ( $\Gamma_4$ ) ordering was found for all compounds at RT, as previously informed for  $\text{LuFe}_{0.5}\text{Cr}_{0.5}\text{O}_3$  [6].

#### B. Magnetization measurements

ZFC and FC magnetization curves measured under an applied magnetic field of 100 Oe increasing temperature for all the perovskites with a single thermal treatment at  $1100^\circ\text{C}$  for 12 h are shown in Fig. 2. In the case of  $\text{LuFe}_{0.55}\text{Cr}_{0.45}\text{O}_3$  [Fig. 2(b)], the magnetic order begins at  $T_N \sim 350$  K with a FC magnetic susceptibility maximum at 270 K and  $T_{\text{comp}} = 195$  K. Meanwhile,  $\text{LuFe}_{0.45}\text{Cr}_{0.55}\text{O}_3$  [Fig. 2(a)] shows a  $T_N \sim 277$  K, and FC magnetic susceptibility drops and crosses the

TABLE II. Magnetic moment components  $M_x$ ,  $M_y$ , and  $M_z$  and magnetic moment module obtained from NPD at 300 K for  $\text{LuFe}_{1-x}\text{Cr}_x\text{O}_3$  with  $x = 0.25, 0.45, 0.55$ , and  $0.75$ . During the refinements, the refined  $M_y$  and  $M_z$  components were close to zero with large standard deviation, and thus, they were supposed null and were fixed to zero in the final refinements.

	$\text{LuFe}_{0.75}\text{Cr}_{0.25}\text{O}_3$	$\text{LuFe}_{0.55}\text{Cr}_{0.45}\text{O}_3$	$\text{LuFe}_{0.45}\text{Cr}_{0.55}\text{O}_3$	$\text{LuFe}_{0.25}\text{Cr}_{0.75}\text{O}_3$
$\text{Fe}^{3+}/\text{Cr}^{3+}$ sublattice				
$M_x$	2.84 (2)	1.45 (2)	0.86 (7)	0.53 (5)
$M_y$	0	0	0	0
$M_z$	0	0	0	0
$ M $	2.84 (2)	1.45 (2)	0.86 (7)	0.53 (5)

zero value at  $T_{\text{comp}} = 225$  K. As  $\text{Lu}^{3+}$  is a diamagnetic cation, the observed magnetization is only due to  $\text{Fe}^{3+}$  and  $\text{Cr}^{3+}$  cations. For reference, the magnetic moments of the transition metal sublattice order as AFM at  $T_N = 628$  K in  $\text{LuFeO}_3$  [31] and at  $T_N = 115$  K for  $\text{LuCrO}_3$  [32].  $\text{LuFe}_{0.75}\text{Cr}_{0.25}\text{O}_3$  was excluded from Fig. 2 because its  $T_N$  is much higher than the temperature limit of the experiment (400 K).

In the case of  $\text{LuFe}_{0.25}\text{Cr}_{0.75}\text{O}_3$  [Fig. 2(c)], in addition to the first thermal treatment at  $1100^\circ\text{C}$ , we also performed additional thermal treatments at  $1250$  and  $1350^\circ\text{C}$ . Strikingly, we can observe MR in Fig. 2(c), which is not expected at this composition [19,23,27] ( $T_{\text{comp}} \sim 55 - 80$  K and  $T_N \sim 150$  K). Moreover, MR disappears after the second thermal treatment at  $1350^\circ\text{C}$  in some of the samples (see Fig. S3 in the Supplemental Material [1]). However, the peak in the magnetization below  $T_N$  remains after the second thermal treatments. Finally, we point out that, under an intermediate

thermal treatment at  $1250^\circ\text{C}$ , this sample still shows MR, and the other samples are not particularly affected.

In a previous paper, we showed [23] that, for  $\text{LuFe}_{0.60}\text{Cr}_{0.40}\text{O}_3$ , below the Néel temperature, the WFM component of  $\text{Fe}^{3+}$  ions aligns in the direction of the applied magnetic field, while the WFM component of the  $\text{Cr}^{3+}$  ions is opposite to the magnetic field. This mechanism is responsible for the appearance of MR [23], which is suppressed at higher  $H$  values. The weak component of the magnetic moments of  $\text{Fe}^{3+}$  and  $\text{Cr}^{3+}$  cannot be antiparallel under strong fields, and hence, the WFM components all point in the direction of the field. In other words, the weak *ferrimagnetic* (FiM) state is broken [27], and then MR disappears. Particularly, it is worth stressing that Fe- and Cr-rich compositions should not show MR because the cation-rich contribution on the magnetization is dominant, and the compensation necessary for MR is not expected [23].

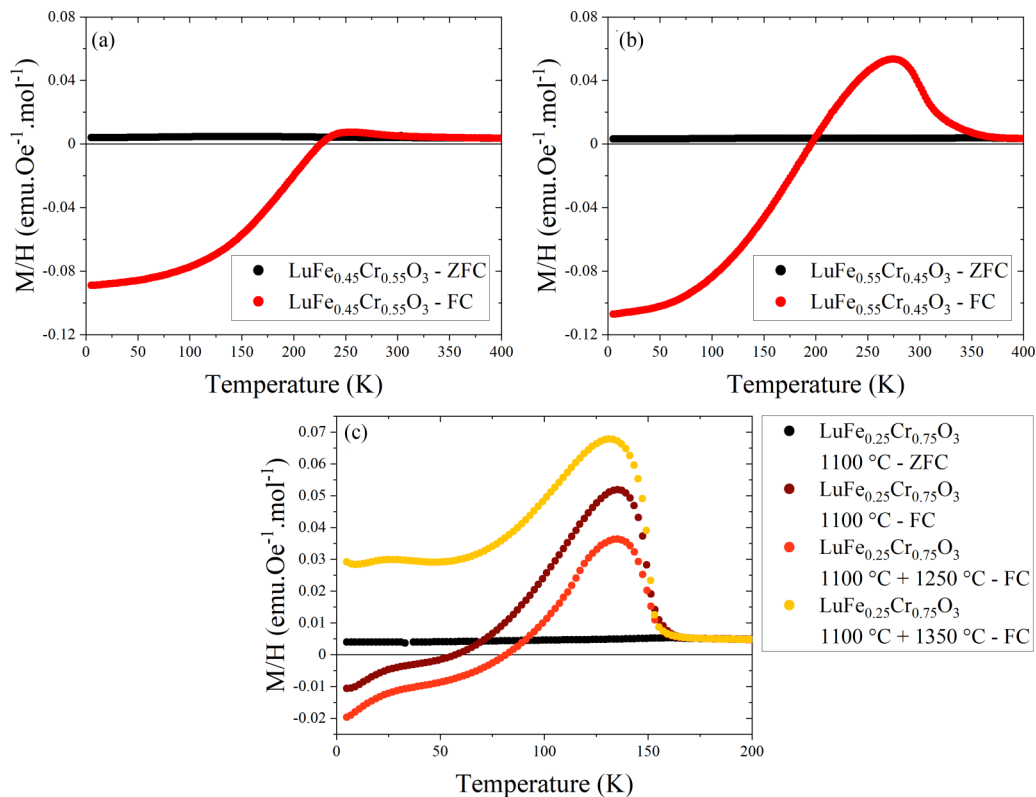


FIG. 2. (a) and (b) magnetization curves of the  $\text{LuFe}_{1-x}\text{Cr}_x\text{O}_3$  perovskites synthesized at  $1100^\circ\text{C}$  as a function of temperature measured at  $H = 100$  Oe. (c) Samples with additional thermal treatments at  $1250$  and  $1350^\circ\text{C}$ .

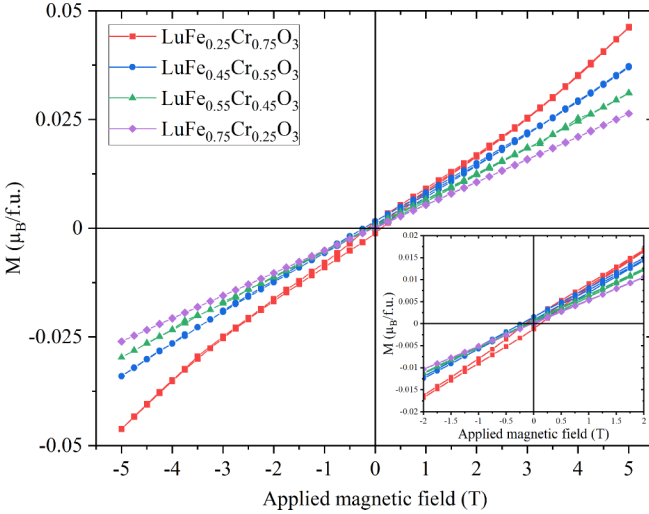


FIG. 3. Isothermal magnetization curves for  $\text{LuFe}_{1-x}\text{Cr}_x\text{O}_3$  samples measured at  $T = 5$  K. The inset shows a zoom of the low magnetic field zone. Red squares:  $\text{LuFe}_{0.25}\text{Cr}_{0.75}\text{O}_3$ ; blue circles:  $\text{LuFe}_{0.45}\text{Cr}_{0.55}\text{O}_3$ ; green triangles:  $\text{LuFe}_{0.55}\text{Cr}_{0.45}\text{O}_3$ ; violet diamonds:  $\text{LuFe}_{0.75}\text{Cr}_{0.25}\text{O}_3$ .

Isothermal magnetization measurements as a function of applied magnetic field are shown in Fig. 3. All the compositions (except  $\text{LuFe}_{0.75}\text{Cr}_{0.25}\text{O}_3$ ) display a hysteresis loop consistent with a WFM behavior [6]. The magnetization at the maximum field (5 T) increases with the content of  $\text{Cr}^{3+}$ . This is because the contribution to the canted magnetization of  $\text{Cr}^{3+}\text{-O}^{2-}\text{-Cr}^{3+}$  superexchange interactions is higher (at low temperatures) than the contribution of  $\text{Fe}^{3+}\text{-O}^{2-}\text{-Fe}^{3+}$  ones.

#### IV. MC SIMULATIONS

##### A. General simulation principles

We modeled  $\text{LuFe}_{1-x}\text{Cr}_x\text{O}_3$  perovskites for several values of  $x$  using a classical Heisenberg model with magnetic moments embedded in a cubic lattice with  $N = (L \times L \times L)$  sites,

$$\mathcal{H} = \sum_{\langle i,j \rangle} [J_{ij} \mathbf{S}_i \cdot \mathbf{S}_j + \mathbf{D}_{ij} \cdot (\mathbf{S}_i \times \mathbf{S}_j)] - \sum_i K_i (\mathbf{S}_i^x)^2 - H \sum_i m_i \mathbf{S}_i^z, \quad (1)$$

where  $\mathbf{S}_i$  are unitary magnetic vectors associated with the magnetic moment of the cation in site  $i$  of the cubic lattice and  $\mathbf{S}_i^x$  and  $\mathbf{S}_i^z$  are the  $x$  and  $z$  components of these magnetic vectors, respectively. The first term corresponds to the pair interactions,  $J_{ij}$  and  $\mathbf{D}_{ij}$  where  $\langle i, j \rangle$  refers to a sum over nearest neighbor sites.  $J_{ij} < 0$  is the superexchange AFM interaction, and the vectors  $\mathbf{D}_{ij}$  account for the antisymmetric DM interactions. Both pair interactions,  $J_{ij}$  and  $D_{ij} = |\mathbf{D}_{ij}|$

depend on the type of ions ( $\text{Fe}^{3+}$  or  $\text{Cr}^{3+}$ ) that occupy sites  $i$  and  $j$ , which means that each pair interaction can take three different values. For instance, if we define 1 as a site occupied by  $\text{Cr}^{3+}$  and 2 as a site occupied by  $\text{Fe}^{3+}$ , then the superexchange interaction couplings are  $J_{11} = 2S_{\text{Cr}}^2 J_{\text{CrCr}}/k_B$ ,  $J_{12} = J_{21} = 2S_{\text{Fe}} S_{\text{Cr}} J_{\text{FeCr}}/k_B$ , and  $J_{22} = 2S_{\text{Fe}}^2 J_{\text{FeFe}}/k_B$ , where  $J_{\alpha\beta}$  (with  $\alpha, \beta = \text{Cr}$  or  $\text{Fe}$ ) are the exchange integrals and  $k_B$  is the Boltzmann constant. Similarly, for the modules of the DM vectors, we have  $D_{11} = S_{\text{Cr}}^2 D_{\text{CrCr}}/k_B$ ,  $-D_{12} = D_{21} = S_{\text{Fe}} S_{\text{Cr}} D_{\text{FeCr}}/k_B$ , and  $D_{22} = S_{\text{Fe}}^2 D_{\text{FeFe}}/k_B$ . The second and third terms correspond to the single site interactions, i.e., the single site anisotropy. In the second, we have the uniaxial anisotropies  $K_1 = S_{\text{Cr}} K_{\text{Cr}}/k_B = K_2 = S_{\text{Fe}} K_{\text{Fe}}/k_B > 0$ , according to our choice that the anisotropy term aligns with the AFM ordering in the  $x$  direction where, for simplicity, we consider here the same anisotropy for  $\text{Cr}^{3+}$  and  $\text{Fe}^{3+}$  ions. Notice that the canting angle is mainly dominated by DM and superexchange interactions. Then for MR, the magnitude of the single site anisotropy is not very important. Finally, the third term corresponds to the Zeeman coupling, where  $H$  is the component in the  $z$  direction of the applied magnetic field. Here,  $H$  is expressed for convenience as  $H = B\mu_{\text{Fe}}/k_B$ , where  $B$  is the external field expressed in conventional units,  $\mu_{\text{Fe}} = g\mu_B S_{\text{Fe}}$  with  $g = 2$  (gyromagnetic factor), and  $\mu_B$  the Bohr magneton. Expressed in this way, the magnetic field is in units of Kelvin, and in addition, the magnetic moments of the ions are measured in terms of the magnetic moments of  $\text{Fe}^{3+}$ . Considering that  $S_{\text{Fe}} = 5/2$  is the total spin of the  $\text{Fe}^{3+}$  ion and  $S_{\text{Cr}} = 3/2$  for the  $\text{Cr}^{3+}$  ion, then in these units,  $m_i = 1$  for  $\text{Fe}^{3+}$  ions, and  $m_i = S_{\text{Cr}}/S_{\text{Fe}} = 0.6$  for  $\text{Cr}^{3+}$  ions. This model uses the minimal ingredients to emulate our system and has been tested in a previous paper [23] in which we were able to reproduce with good accuracy the Néel temperature as a function of composition in  $\text{LuFe}_{1-x}\text{Cr}_x\text{O}_3$  and  $\text{YFe}_{1-x}\text{Cr}_x\text{O}_3$ . For more details on the implementation, setting of the parameters, and validation of the approach, see Ref. [23] and references therein. In Table III, we show the magnitude of all the parameters used in MC simulation.

To understand the experimental results previously shown, we have performed MC simulations using cubic lattices of sizes  $L = 40$  and  $60$  having  $N = 64\,000$  and  $216\,000$  magnetic moments, respectively. Two types of systems were used: *homogeneous* and *inhomogeneous* systems. In homogeneous systems, each site of the cubic lattice is randomly occupied by  $\text{Cr}^{3+}$  or  $\text{Fe}^{3+}$  ions with a probability that keeps the nominal overall compositional ratio. In inhomogeneous cases, the composition of the system fluctuates around a mean value in each length scale. To implement this setup, the cube is divided in eight octants, where each octant has its own overall composition, and inside each octant, every site is randomly occupied by  $\text{Cr}^{3+}$  and  $\text{Fe}^{3+}$  ions with a probability that keeps the given overall compositional ratio for this octant. The mean compositional ratio of the whole system is equal to the overall

TABLE III. Parameters used in the Monte Carlo simulations. Definitions in text.

$J$ [K]	$J_{22}$ [K]	$J_{11}$ [K]	$J_{12}$ [K]	$D_{22}$ [K]	$D_{11}$ [K]	$D_{12}$ [K]	$K_2$ [K]	$K_1$ [K]	$H$ [K]
436	J	0.183 J	0.243 J	$2.14 \times 10^{-2}$ J	$0.74 \times 10^{-2}$ J	$-1.70 \times 10^{-2}$ J	$0.70 \times 10^{-2}$ J	$0.70 \times 10^{-2}$ J	$0.20 \times 10^{-2}$ J

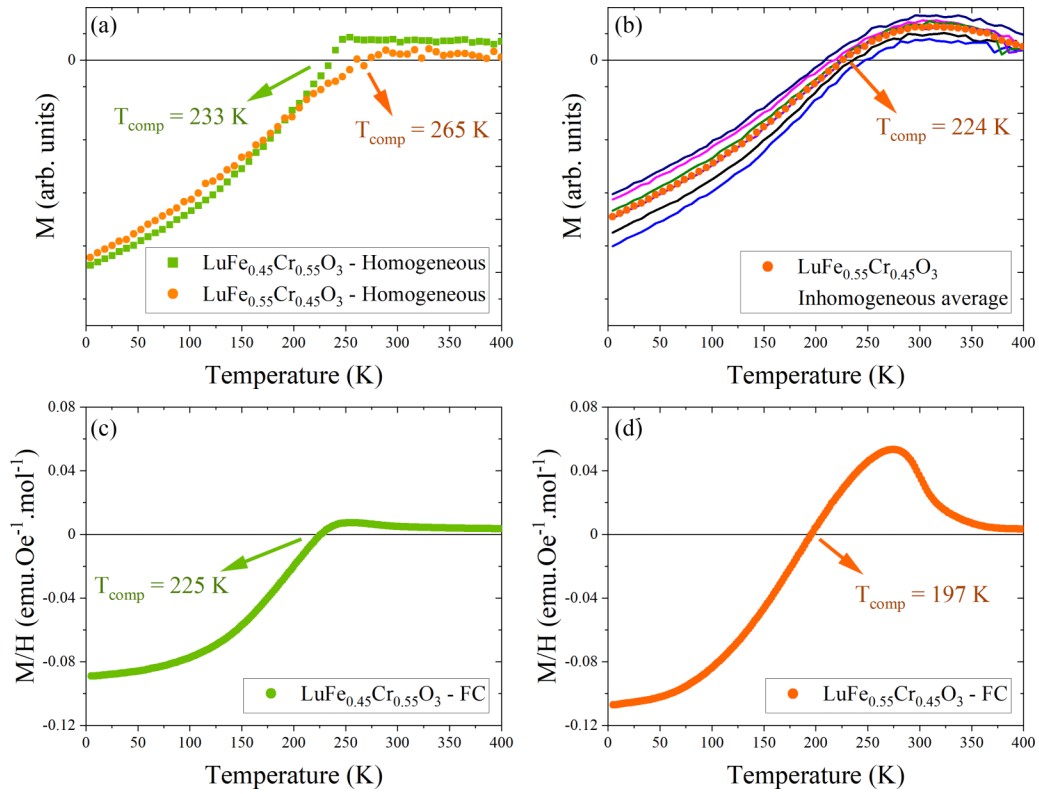


FIG. 4. (a) FC curves of the homogeneous systems  $\text{LuFe}_{0.55}\text{Cr}_{0.45}\text{O}_3$  and  $\text{LuFe}_{0.45}\text{Cr}_{0.55}\text{O}_3$  obtained by MC simulations. (b) FC curves of the inhomogeneous system for  $\text{LuFe}_{0.55}\text{Cr}_{0.45}\text{O}_3$ , where lines correspond to single realizations and dots to the average of these curves. The experimental FC curves for (c)  $\text{LuFe}_{0.45}\text{Cr}_{0.55}\text{O}_3$  and (d)  $\text{LuFe}_{0.55}\text{Cr}_{0.45}\text{O}_3$ .

nominal composition. For simplicity, to run MC simulations, the shape of these octants is ideally cubic and periodic, but this kind of shape and periodicity is not expected in real samples.

Heterogeneous distributions of magnetic cations have been frequently correlated with unusual magnetic properties in crystalline materials. A phenomenological model of magnetic clusters in perovskites was proposed to describe the unusual magnetic relaxation behavior in  $\text{CaLaFeSnO}_6$  [33]. Also, the existence of two types of uncompensated WFM clusters distributed on an AFM matrix has been proposed to explain the magnetic behavior in  $\text{Fe}_{0.67}\text{Cr}_{0.33}\text{F}_3$  [34]. Moreover, cluster formation in perovskite solid solutions or double perovskites has been explored recently to describe different experimentally observed magnetic phenomena [35–38]. For example, superparamagnetism in double perovskite  $\text{Ba}_{1+x}\text{La}_{1-x}\text{MnSbO}_6$  with  $0.1 \leq x \leq 0.7$  can be explained by the formation of three-dimensional nanoclusters formed by regions rich in  $\text{Mn}^{2+} - \text{O}^{2-} - \text{Mn}^{2+}$  superexchange paths [39,40]. In addition, recent studies show that MR in  $\text{La}_{1-x/2}\text{Bi}_{x/2}\text{Fe}_{0.5}\text{Cr}_{0.5}\text{O}_3$  perovskites is due to canted WFM domains and clusters richer in chromium or iron AFM coupled through  $\text{Cr}^{3+} - \text{O} - \text{Fe}^{3+}$  interactions [41].

Finally, in  $\text{LaFe}_{0.5}\text{Cr}_{0.5}\text{O}_3$  perovskites, it was shown by Coutinho *et al.* [20] that MR is affected by thermal treatments. The authors of this study proposed that thermal treatments at high temperature induce oxygen vacancy and volatilization of La and that this produces different valence states in the transition metals and consequently new superexchange and DM interactions. Hence, thermal treatments induce MR by a differ-

ent mechanism than cluster formation. However, lanthanum volatilization is not probable due to  $\text{La}_2\text{O}_3$  high melting and boiling points, and  $\text{Lu}^{3+}$  and  $\text{O}^{2-}$  vacancies are not formed in our samples (and  $\text{Lu}_2\text{O}_3$  in our case), as observed in NPD refinements.

In summary, inhomogeneities such as clusters may be necessary to explain several magnetic behaviors in perovskites, particularly the MR phenomenon. These inhomogeneities can be influenced by the different thermal treatments and processing routes of the material. However, clusters have not been directly observed yet due to experimental and technical limitations.

## B. MC simulations results

In Fig. 4(a), FC magnetization curves of  $\text{LuFe}_{1-x}\text{Cr}_x\text{O}_3$  obtained by numerical simulations are shown for  $x = 0.45$  and  $0.55$  with a homogeneous system of  $L = 40$ . MR is observed in both cases, although the peak in the magnetization before MR is absent, and both  $T_{\text{comp}}$  are lower than in experiments. Particularly for  $x = 0.45$ , the discrepancy with experiments is more remarkable; for this reason, we explored the effect of spatial fluctuations on this specific composition. The FC curves obtained for the inhomogeneous system with  $x = 0.45$  are shown in Fig. 4(b). In this specific case, the size of the system  $N$  was increased because, in an inhomogeneous setup, the curves are fluctuating more due to disorder effects, such as the heterogeneities in the distribution of the ions and small variations of the sample composition at each realization; hence,

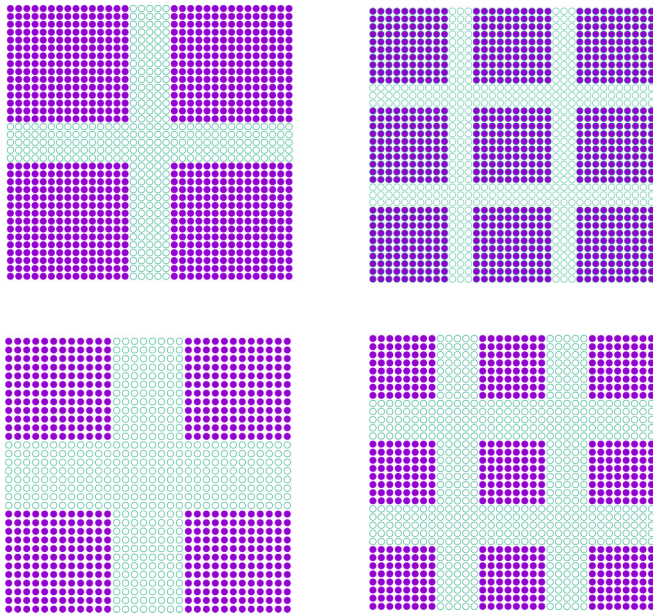


FIG. 5. In-plane projection of a cube with eight clusters (left) and 27 clusters (right) with the following compositions:  $\text{LuFe}_{0.45}\text{Cr}_{0.55}\text{O}_3$  (top panels) and  $\text{LuFe}_{0.25}\text{Cr}_{0.75}\text{O}_3$  (bottom panels). Filled circles correspond to  $\text{Fe}^{3+}$  ions and empty circles to  $\text{Cr}^{3+}$  ions.

we set  $L = 60$ . The composition of each octant is randomly chosen from the interval  $[x - \Delta x, x + \Delta x]$  with  $\Delta x = 0.35$  in a way that the global composition is kept nearly constant and equal to the experimental value. It is worth mentioning that, as  $\Delta x$  increases, starting from zero, the size of the peak before MR increases as does the ordering temperature  $T_N$ .

Meanwhile,  $T_{\text{comp}}$  decreases. In Fig. 4(b), the lines correspond to single realizations of MC simulations and the dots to the averaged curves over all realizations. A single MC realization implies both a new thermal running and a new draw in the distribution of the ions. In these new simulations, a peak appears in magnetization before MR, and  $T_{\text{comp}}$  decreases, approaching the experimental results. For comparison, we also include the experimental FC curves for  $\text{LuFe}_{0.45}\text{Cr}_{0.55}\text{O}_3$  and  $\text{LuFe}_{0.55}\text{Cr}_{0.45}\text{O}_3$ , Figs. 4(c) and 4(d), respectively.

### C. Multicluster MC simulations

Motivated by the results obtained in  $\text{LuFe}_{0.25}\text{Cr}_{0.75}\text{O}_3$ , we now explore the effect of cluster formation on the magnetic properties by MC simulation, focusing on samples that are rich in chromium. The appearance of MR at  $x = 0.75$  cannot be explained with MC simulations, even using inhomogeneous setups. This poses the question about the existence of well-defined  $\text{Fe}^{3+}$  clusters embedded in a  $\text{Cr}^{3+}$  matrix. To keep the system as simple as possible to run the MC simulations, we consider cubic clusters entirely composed of  $\text{Fe}^{3+}$  ions. Two compositions were explored in this way  $x = 0.55$  and  $0.75$ , and for each composition, two cluster configurations were tested: one with eight clusters and another with 27 clusters. To visualize how cluster separation depends on the number of clusters and composition, the four system configurations are shown in Fig. 5.

MC results for FC curves are shown in Fig. 6 for the clustered systems. For clarity reasons, only the case for  $x = 0.75$  is analyzed here. The results for  $x = 0.55$  are included in Fig. S4 of the Supplemental Material [1]. Figures 6(b) and 6(c) show several MC realizations of FC curves for systems

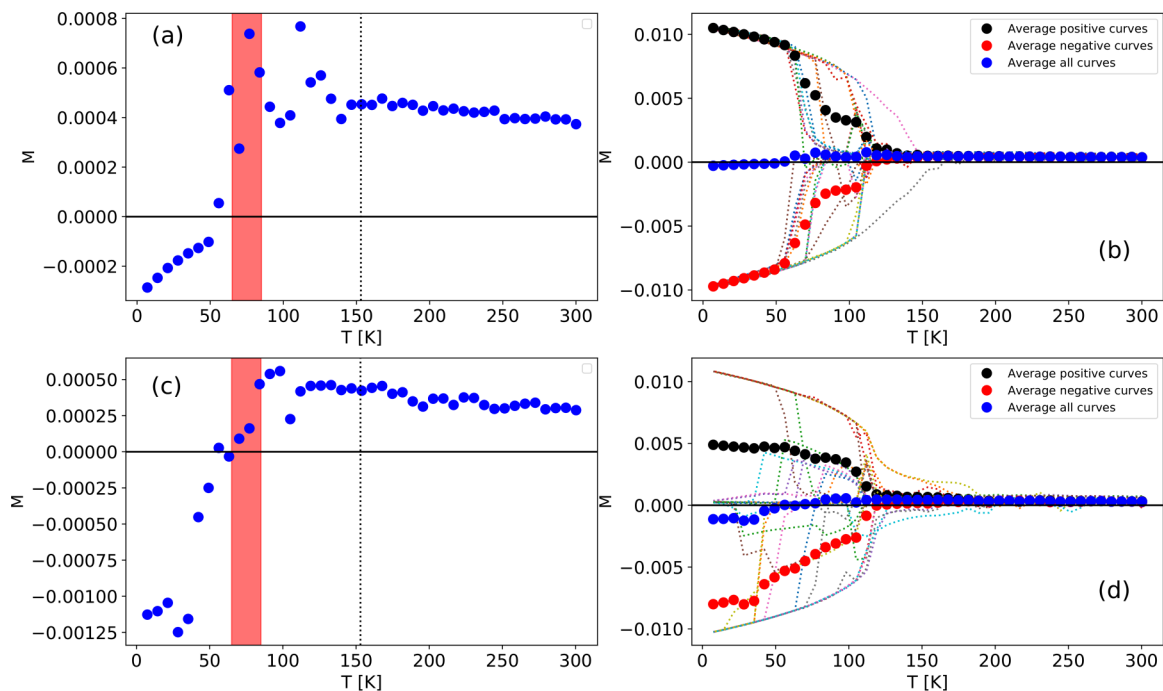


FIG. 6. Simulated FC magnetization for clustered  $\text{LuFe}_{0.25}\text{Cr}_{0.75}\text{O}_3$ . Top panels correspond to eight clusters and bottom panels to 27 clusters. (a) and (c) Averaged curves over 30 realizations. The pink shadow bar indicates the range of compensation temperatures observed in experiments. (b) and (d) Individual realizations of FC curves (lines) showing also averages (dots) over positive and negative curves.

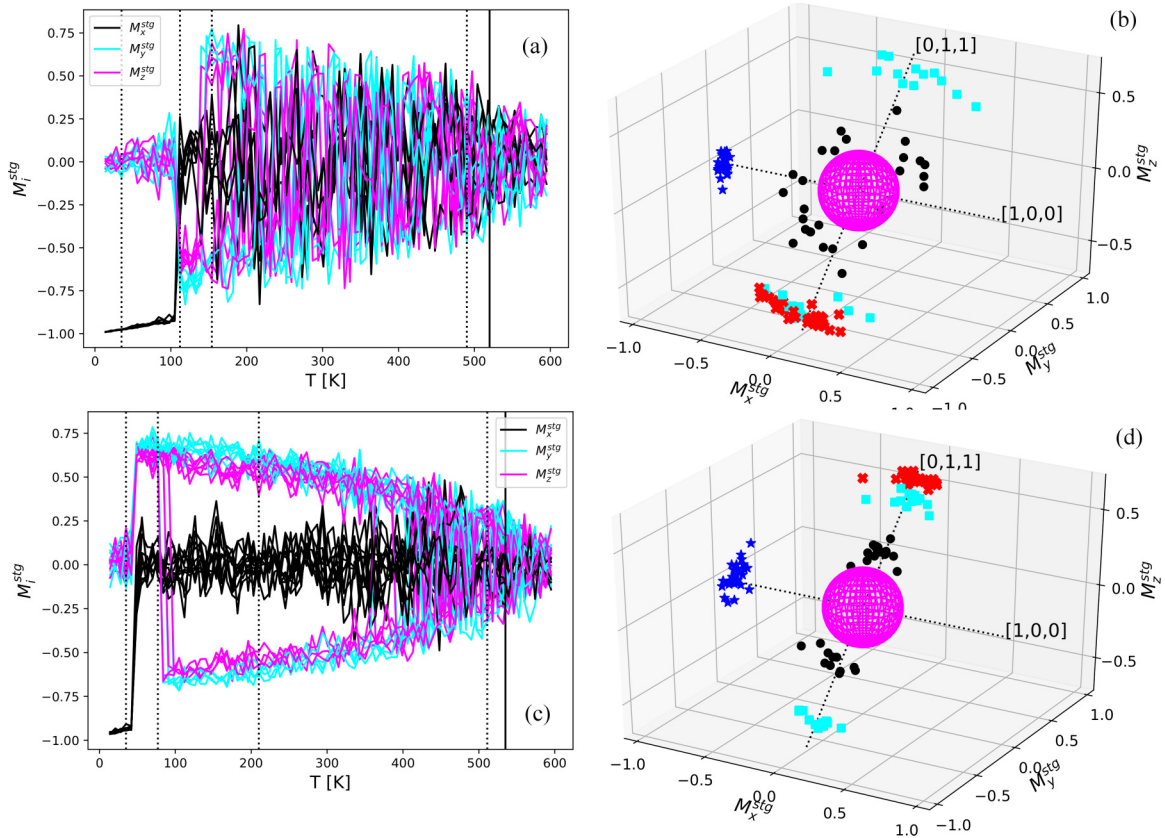


FIG. 7. Components of the staggered magnetization  $M^{\text{stg}}$  as a function of the temperature of 10 individual clusters selected of two systems having 27 clusters: (a)  $\text{LuFe}_{0.25}\text{Cr}_{0.75}\text{O}_3$  and (c)  $\text{LuFe}_{0.45}\text{Cr}_{0.55}\text{O}_3$ . The full vertical lines indicate the ordering temperature of the clusters which are 520 and 535 K, for (a) and (c), respectively (see Fig. S4 of the Supplemental Material [1] for details). (b) and (d)  $M^{\text{stg}}$  for each individual cluster of the system at four selected temperatures that are indicated by dashed lines in (a) and (c). At high temperature (black circles), both systems are superparamagnetic. As temperature decreases, the clusters are oriented in both  $[011]$  and  $[0\bar{1}\bar{1}]$  directions in a nearly frozen state (cyan squares). As temperature decreases even more, all the clusters are oriented in the same direction ( $[011]$  or  $[0\bar{1}\bar{1}]$ ) in a frozen state (red crosses). Finally, at a low enough temperature, all rotate, as expected, to the easy direction  $[100]$  (blue stars).

with large (8) and small (27) clusters. Strong fluctuations are observed in the magnetization in each realization, and the realizations differ among them. Some of them do not show MR. Since clustered systems are highly heterogeneous, strong fluctuations are expected due to size effects. In particular, the fluctuations are larger for systems with eight clusters, i.e., the more heterogeneous system in this size scale. The averaged curves, however, show MR in both large and small clusters. In the case of small clusters, a peak is observed before the reversal, as observed in the experiments. However,  $T_{\text{comp}}$  and  $T_N$  are smaller:  $\sim 50$  and  $\sim 125$  K, respectively, as compared with the values obtained from Fig. 2. This indicates that the size of the cluster is important to define the shape of the FC curve, and particularly for the presence of the peak in magnetization before MR. A similar behavior is observed in systems with  $x = 0.55$  as it is shown in the Supplemental Material [1] (Fig. S4).

An interesting aspect of these clustered systems is that the clusters are composed of  $\text{Fe}^{+3}$  ions, hence ordering as AFM at a higher temperature than the matrix composed of  $\text{Cr}^{+3}$  ions. However, once the iron clusters are ordered, thermal fluctuations at high temperature should prevent a preferential direction for the AFM ordering, as observed at high temperature in common superparamagnetic systems. Instead of ferromagnetic nanoparticles or clusters whose magnetization

reverse by thermal fluctuations [42,43], here, we have small AFM clusters rich in iron with the staggered magnetization randomly oriented by thermal agitation.

To explore this effect, we have analyzed the magnetic behavior of the individual iron clusters embedded in the matrix. Since clusters are mainly AFM ordered, having only a WFM magnetization, we evaluate the staggered magnetization. The WFM due to DM interactions is difficult to detect at high temperatures because this is a highly fluctuating magnitude, especially in small clusters due to size effects. Figure 7 shows the components of the staggered magnetization of each cluster in the chromium matrix as a function of the temperature in a FC process.

Two setups with 27 clusters and different compositions are shown; Fig. 7(a) corresponds to  $\text{LuFe}_{0.45}\text{Cr}_{0.55}\text{O}_3$  and Fig. 7(b) to  $\text{LuFe}_{0.25}\text{Cr}_{0.75}\text{O}_3$ . Each composition has a different cluster size and separation (see Fig. 5). However, a superparamagnetic behavior is observed in both cases.

At high temperatures, the staggered magnetization components of each cluster strongly fluctuates, indicating that clusters are in a superparamagnetic state. At low temperatures,  $\sim 130$  and  $\sim 400$  K for  $x = 0.75$  and  $0.55$ , respectively, the clusters get blocked, and all aligned in  $[011]$  directions. Remarkably, this is not the easy axis direction ( $x$  direction



or [001]), see Figs. 7(b) and 7(d). At low intermediate temperatures, the clusters somehow order due to interaction with the matrix, pointing all the same direction ([011] or  $[0\bar{1}\bar{1}]$ ). Finally, at a low enough temperature, the clusters rotate toward the easy axis direction, and simultaneously, the chromium matrix orders as AFM with the spins also aligned in the easy axis direction. This spin reorientation transition is related to a metastable state due maybe to size effects or the short time dynamics of MC simulation, but these assumptions require further analysis.

The ordering temperature of the clusters ( $T_N^{\text{Clus}}$ ) and the matrix ( $T_N^{\text{Mat}}$ ) can be determined in MC simulations calculating the specific heat (see Fig. S5 in the Supplemental Material [1]). We found that, in both compounds, the clusters order at nearly the same temperature  $T_N^{\text{Clus}} \sim 520$  and  $535$  K for  $x = 0.75$  and  $0.55$ , respectively, while the matrix orders at  $T_N^{\text{Mat}} \sim 115$  K. There is considerable reduction in the cluster ordering temperature as compared with the bulk, as  $T_N \sim 628$  K for  $\text{LuFeO}_3$ , while the matrix orders at the expected temperature as  $T_N \sim 115$  K for  $\text{LuCrO}_3$ .

## V. DISCUSSION

MC simulations showed that the FC curves measured in  $\text{LuFe}_{1-x}\text{Cr}_x\text{O}_3$  can be reproduced by introducing inhomogeneity in the distribution of  $\text{Fe}^{3+}$  and  $\text{Cr}^{3+}$  cations. Homogeneous setups cannot emulate, for instance, the peak that appears in FC magnetization curves before the compensation temperature in  $\text{LuFe}_{0.55}\text{Cr}_{0.45}\text{O}_3$ . Also, at this composition, the  $T_{\text{comp}}$  obtained by MC simulations is considerably lower than in the experiments. When spatial fluctuations of the composition are introduced in MC setups, the peak preceding MR appears and  $T_{\text{comp}}$  rises, approaching the experimental values. MC simulation results suggest that the annealing at high temperatures modifies the distribution of  $\text{Fe}^{3+}$  and  $\text{Cr}^{3+}$  cations in the samples, for instance, the size of the clusters or, in a more general way, the length scale at which the variation in composition takes place.

In a previous paper, we had reported [23] that a peak appears in homogeneous systems only for  $x \leq 0.4$  and in a narrow range. Here, we have shown that by introducing spatial fluctuations in the composition, i.e., using an inhomogeneous setup, it is possible to extend the upper limit in composition under which this peak is observed. However, the unexpected appearance of MR in  $\text{LuFe}_{0.25}\text{Cr}_{0.75}\text{O}_3$  cannot be explained by the introduction of continuous modulations in the composition (inhomogeneous system). Instead, the observed behavior could be modeled by adding small clusters in MC setups. The ordering temperature of the clusters  $T_N^{\text{Clus}}$  and the matrix  $T_N^{\text{Mat}}$  was determined by MC simulations calculating the specific heat. We found that, in  $\text{LuFe}_{0.45}\text{Cr}_{0.55}\text{O}_3$  and  $\text{LuFe}_{0.25}\text{Cr}_{0.75}\text{O}_3$ , the clusters order at nearly the same temperature  $T_N^{\text{Clus}} \sim 520$  and  $535$  K for  $x = 0.75$  and  $0.55$ , respectively, while the matrix orders at  $T_N^{\text{Mat}} \sim 115$  K. There is considerable reduction in the cluster ordering temperature

as compared with the bulk, as  $T_N \sim 628$  K for  $\text{LuFeO}_3$ , while the matrix orders at the expected temperature as  $T_N \sim 115$  K for  $\text{LuCrO}_3$ . In this case, the staggered magnetization of the  $\text{Fe}^{3+}$  clusters embedded in the  $\text{Cr}^{3+}$  matrix fluctuate at high temperatures. In other words, there is a regime at high temperatures where clusters are in a superparamagnetic state. Finally, at a lower enough temperature, all rotate, as expected, to the easy direction [100], and an AFM state is obtained.

## VI. CONCLUSIONS

We have shown that, in the  $\text{LuFe}_{1-x}\text{Cr}_x\text{O}_3$  solid solution, MR is observed for  $0.45 \leq x \leq 0.75$ . For  $x = 0.75$ , the appearance of MR is highly dependent on the thermal treatment and synthesis process of the sample. We could explain all the phenomena by using MC simulations. However, we are aware that our MC model introduces several simplifications and is restricted to small system sizes due to computational limitations. Moreover, different modulation scales in the composition and the dispersion in cluster sizes are not considered in our analysis. However, this simplified model for  $\text{LuFe}_{1-x}\text{Cr}_x\text{O}_3$  perovskite solid solutions captures many of the relevant features observed in FC experiments. We conclude that inhomogeneity in the distribution of  $\text{Cr}^{3+}$  and  $\text{Fe}^{3+}$  improves the agreement between experimental FC curves and MC simulations. For example, using an inhomogeneous setup, it is possible to extend the upper limit in composition under which the peak in the magnetization below  $T_N$  is observed. The unexpected appearance of MR in  $\text{LuFe}_{0.25}\text{Cr}_{0.75}\text{O}_3$  could not be explained by the introduction of continuous modulations in the composition (inhomogeneous system). Instead, small clusters added to the MC setups could reproduce the experimental results. This is reasonable since an inhomogeneous solid solution would present  $\text{Fe}^{3+}$ - or  $\text{Cr}^{3+}$ -rich regions and a tendency to form magnetic nanoclusters. The formation of magnetic nanoclusters has been overwhelmingly informed in literature [33–40]. The thermal protocol being the same, the rate of heating and cooling should not affect the formation of clusters, if any, which would imply that the different heat treatments and processing of the sample is responsible for the differences in magnetic behavior.

## ACKNOWLEDGMENTS

This paper was partially supported by grants from CONICET, SeCyT–Universidad Nacional de Córdoba, Argentina (No. PIP 112 2015010028), MinCyT Córdoba (No. PID PG 0144/2018), FONCyT (No. PICT-2016-2495), and a CONICET-CNRS cooperation program. F.E.L. and J.P.B. thank CONICET for fellowships. This paper used computational resources from CCAD-UNC, which is part of SNCAD-MinCyT, Argentina. J.P.B., C.M., and A.M. also acknowledge the financial support of the French Agence Nationale de la Recherche LabEx EMC3 through the Project MaPhoObi (Grant No. ANR-10-LABX-09-01), and the Normandy Region (Réseau d'Intérêt Normand—Label d'excellence).

[1] See Supplemental Material at <https://link.aps.org/supplemental/10.1103/PhysRevB.103.014447> for explanatory figures, a table

of Rietveld refinement from XRPD, and additional experimental and MC results on magnetization reversal.

- [2] A. M. Glazer, The classification of tilted octahedra in perovskites, *Acta Cryst. B* **28**, 3384 (1972).
- [3] Y. Fang, Y. Yang, X. Liu, J. Kang, L. Hao, X. Chen, L. Xie, G. Sun, V. Chandragiri, C. Wang, Y. Cao, F. Chen, Y. Liu, D. Chen, S. Cao, C. Lin, W. Ren, and J. Zhang, Observation of re-entrant spin reorientation in  $\text{TbFe}_{1-x}\text{Mn}_x\text{O}_3$ , *Sci. Rep.* **6**, 33448 (2016).
- [4] H. S. Nair, Z. Fu, C. M. N. Kumar, V. Y. Pomjakushin, Y. Xiao, T. Chatterji, and A. M. Strydom, Spin-lattice coupling and frustrated magnetism in Fe-doped hexagonal  $\text{LuMnO}_3$ , *Europhys. Lett.* **110**, 37007 (2015).
- [5] Z. Fu, H. S. Nair, Y. Xiao, A. Senyshyn, V. Y. Pomjakushin, E. Feng, Y. Su, W. T. Jin, and T. Brückel, Magnetic structures and magnetoelastic coupling of Fe-doped hexagonal manganites  $\text{LuMn}_{1-x}\text{Fe}_x\text{O}_3$  ( $0 \leq x \leq 0.3$ ), *Phys. Rev. B* **94**, 125150 (2016).
- [6] F. Pomiro, R. D. Sánchez, G. Cuello, A. Maignan, C. Martin, and R. E. Carbonio, Spin reorientation, magnetization reversal, and negative thermal expansion observed in  $R\text{Fe}_{0.5}\text{Cr}_{0.5}\text{O}_3$  perovskites ( $R = \text{Lu}, \text{Yb}, \text{Tm}$ ), *Phys. Rev. B* **94**, 134402 (2016).
- [7] J. P. Bolletta, F. Pomiro, R. D. Sánchez, V. Pomjakushin, G. Aurelio, A. Maignan, C. Martin, and R. E. Carbonio, Spin reorientation and metamagnetic transitions in  $R\text{Fe}_{0.5}\text{Cr}_{0.5}\text{O}_3$  perovskites ( $R = \text{Tb}, \text{Dy}, \text{Ho}, \text{Er}$ ), *Phys. Rev. B* **98**, 134417 (2018).
- [8] F. Pomiro, D. M. Gil, V. Nassif, A. Paesano Jr., M. I. Gómez, J. Guimpel, R. D. Sánchez, and R. E. Carbonio, Weak ferromagnetism and superparamagnetic clusters coexistence in  $\text{YFe}_{1-x}\text{Co}_x\text{O}_3$  ( $0 \leq x \leq 1$ ) perovskites, *Mater. Res. Bull.* **94**, 472, (2017).
- [9] Ya. B. Bazaliy, L. T. Tsymbal, G. N. Kakazei, A. I. Izotov, and P. E. Wigen, Spin-reorientation in  $\text{ErFeO}_3$ : zero-field transitions, three-dimensional phase diagram, and anisotropy of erbium magnetism, *Phys. Rev. B* **69**, 104429 (2004).
- [10] A. V. Kimel, A. Kirilyuk, A. Tsvetkov, R. V. Pisarev, and Th. Rasing, Laser-induced ultrafast spin reorientation in the antiferromagnet  $\text{TmFeO}_3$ , *Nature* **429**, 850 (2004).
- [11] P. Mandal, C. R. Serrao, E. Suard, V. Caignaert, B. Raveau, A. Sundares, and C. N. R. Rao, Spin reorientation and magnetization reversal in the perovskite oxides,  $\text{YFe}_{1-x}\text{Mn}_x\text{O}_3$  ( $0 \leq x \leq 0.45$ ): a neutron diffraction study, *J. Solid State Chem.* **197**, 408 (2013).
- [12] T. Lottermoser, T. Lonkai, U. Amann, D. Hohlwein, J. Ihringer, and M. Fiebig, Magnetic phase control by an electric field, *Nature* **430**, 541 (2004).
- [13] B. B. Van Aken, T. T. M. Palstra, A. Filippetti, and N. A. Spaldin, The origin of ferroelectricity in magnetoelectric  $\text{YMnO}_3$ , *Nat. Mater.* **3**, 164 (2004).
- [14] R. L. White, Review of recent work on the magnetic and spectroscopic properties of the rare-earth orthoferrites, *J. Appl. Phys.* **40**, 1061 (1969).
- [15] Y. Su, J. Zhang, Z. Feng, L. Li, B. Li, Y. Zhou, Z. Chen, and S. Cao, Magnetization reversal and  $\text{Yb}^{3+}/\text{Cr}^{3+}$  spin ordering at low temperature for perovskite  $\text{YbCrO}_3$  chromites, *J. Appl. Phys.* **108**, 013905 (2010).
- [16] K. Yoshii, Magnetic properties of perovskite  $\text{GdCrO}_3$ , *J. Solid State Chem.* **159**, 204 (2001).
- [17] A. Kumar and S. M. Yusuf, The phenomenon of negative magnetization and its implications, *Phys. Rep.* **556**, 1 (2015).
- [18] J. Mao, Y. Sui, X. Zhang, Y. Su, X. Wang, Z. Liu, Y. Wang, R. Zhu, Y. Wang, W. Liu, and J. Tang, Temperature- and magnetic-field-induced magnetization reversal in perovskite  $\text{YFe}_{0.5}\text{Cr}_{0.5}\text{O}_3$ , *Appl. Phys. Lett.* **98**, 192510 (2011).
- [19] N. Dasari, P. Mandal, A. Sundaresan, and N. S. Vidhyadhiraja, Weak ferromagnetism and magnetization reversal in  $\text{YFe}_{1-x}\text{Cr}_x\text{O}_3$ , *Europhys. Lett.* **99**, 17008 (2012).
- [20] P. Coutinho and P. Barrozo, Influence of the heat treatment on magnetization reversal of orthorhombic perovskites  $\text{LaFe}_{0.5}\text{Cr}_{0.5}\text{O}_3$ , *Appl. Phys. A* **124**, 668 (2018).
- [21] D. Treves, Magnetic studies of some orthoferrites, *Phys. Rev.* **125**, 1843 (1962).
- [22] T. Moriya, New Mechanism of Anisotropic Superexchange Interaction, *Phys. Rev. Lett.* **4**, 228 (1960).
- [23] O. V. Billoni, F. Pomiro, S. A. Cannas, C. Martin, A. Maignan, and R. E. Carbonio, Magnetization reversal in mixed ferrite-chromite perovskites with nonmagnetic cation on the A-site, *J. Phys.: Condens. Matter* **28**, 476003 (2016).
- [24] A. K. Murtazaev, I. K. Kamilov, and Z. G. Ibaev, Monte Carlo study of the critical properties of yttrium orthoferrite, *Low Temp. Phys.* **31**, 139 (2005).
- [25] E. Restrepo-Parra, C. M. Bedoya-Hincapie, J. F. Jurado, J. C. Riaño-Rojas, and J. Restrepo, Monte Carlo study of the critical behavior and magnetic properties of  $\text{La}_{2/3}\text{Ca}_{1/3}\text{MnO}_3$  thin films, *J. Magn. Magn. Mater.* **322**, 3514 (2010).
- [26] E. Restrepo-Parra, C. D. Salazar-Enríquez, J. Londoño-Navarro, J. F. Jurado, and J. Restrepo, Magnetic phase diagram simulation of  $\text{La}_{1-x}\text{Ca}_x\text{MnO}_3$  system by using Monte Carlo, metropolis algorithm and Heisenberg model, *J. Magn. Magn. Mater.* **323**, 1477 (2011).
- [27] I. Fita, V. Markovich, A. S. Moskvin, A. Wisniewski, R. Puzniak, P. Iwanowski, C. Martin, A. Maignan, R. E. Carbonio, M. U. Gutowska, A. Szewczyk, and G. Gorodetsky, Reversed exchange-bias effect associated with magnetization reversal in the weak ferrimagnet  $\text{LuFe}_{0.5}\text{Cr}_{0.5}\text{O}_3$ , *Phys. Rev. B* **97**, 104416 (2018).
- [28] A. Dahmani, M. Taibi, M. Noguez, J. Aride, E. Loudghiri, and A. Belayachi, Magnetic properties of the perovskite compounds  $\text{YFe}_{1-x}\text{Cr}_x\text{O}_3$  ( $0.5 \leq x \leq 1$ ), *Mater. Chem. Phys.* **77**, 912 (2002).
- [29] M. H. Rietveld, A profile refinement method for nuclear and magnetic structures, *J. Appl. Crystallogr.* **2**, 65 (1969).
- [30] J. Rodríguez-Carvajal, Recent advances in magnetic structure determination by neutron powder diffraction, *Physica B* **192**, 55 (1993).
- [31] X.-P. Yuan, Y.-K. Tang, Y. Sun, and M.-X. Xu, Structure and magnetic properties of  $\text{Y}_{1-x}\text{Lu}_x\text{FeO}_3$  ( $0 \leq x \leq 1$ ) ceramics, *J. Appl. Phys.* **111**, 053911 (2012).
- [32] J. R. Sahu, C. R. Serrao, N. Ray, U. V. Waghmare, and C. N. R. Rao, Rare earth chromites: a new family of multiferroics, *J. Mater. Chem.* **17**, 42 (2007).
- [33] T. C. Gibb and R. J. Whitehead, Order-disorder and magnetic clusters in some mixed-metal perovskites, *J. Mater. Chem.* **3**, 591 (1993).
- [34] M. Tamine, M. Noguez, J. L. Dormann, and J. M. Grenèche, Magnetic clustering phenomena in a crystalline mixed ferric fluoride:  $\text{Fe}_{0.67}\text{Cr}_{0.33}\text{F}_3$ , *J. Magn. Magn. Mater.* **140**, 1765 (1995).
- [35] P. D. Battle, T. C. Gibb, A. J. Herod, and J. P. Hodges, Sol-gel synthesis of the magnetically frustrated oxides  $\text{Sr}_2\text{FeSbO}_6$  and  $\text{SrLaFeSnO}_6$ , *J. Mater. Chem.* **5**, 75 (1995).

- [36] P. D. Battle, T. C. Gibb, A. J. Herod, S. Kim, and P. H. Munns, Investigation of magnetic frustration in  $A_2\text{FeMO}_6$  ( $A = \text{Ca}, \text{Sr}, \text{Ba}$ ;  $M = \text{Nb}, \text{Ta}, \text{Sb}$ ) by magnetometry and Mössbauer spectroscopy, *J. Mater. Chem.* **5**, 865 (1995).
- [37] P. Adler, Electronic state, magnetism, and electrical transport behavior of  $\text{Sr}_{3-x}\text{A}_x\text{Fe}_2\text{O}_7$  ( $x \leq 0.4$ ,  $A = \text{Ba}, \text{La}$ ), *J. Solid State Chem.* **130**, 129 (1997).
- [38] D. Franco, R. E. Carbonio, and G. Nieva, Synthesis and structural and magnetic characterization of the frustrated magnetic system  $\text{La}_2\text{Ni}_{4/3-x}\text{Co}_x\text{Sb}_{2/3}\text{O}_6$ , *J. Solid State Chem.* **207**, 69 (2013).
- [39] M. C. Blanco, J. M. De Paoli, S. Ceppi, G. Tirao, V. M. Nassif, J. Guimpel, and R. E. Carbonio, Synthesis, structural characterization and magnetic properties of the monoclinic ordered double perovskites  $\text{BaLaMSbO}_6$ , with  $M = \text{Mn}, \text{Co}$  and  $\text{Ni}$ , *J. Alloys and Comp.* **606**, 139 (2004).
- [40] D. M. Arciniegas Jaimes, M. C. Blanco, F. Pomiro, G. Tirao, V. M. Nassif, G. J. Cuello, J. A. Alonso, and R. E. Carbonio, Synthesis, structural characterization and magnetic properties of the series of double perovskites  $\text{Ba}_{1+x}\text{La}_{1-x}\text{MnSbO}_6$  with  $0.1 \leq x \leq 0.7$ , *J. Alloys and Comp.* **704**, 776 (2017).
- [41] K. Vijayanandhini, Ch. Simon, V. Pralong, Y. Bréard, V. Caignaert, B. Raveau, P. Mandal, A. Sundaresan, and C. N. R. Rao, Zero magnetization in a disordered  $(\text{La}_{1-x/2}\text{Bi}_{x/2})(\text{Fe}_{0.5}\text{Cr}_{0.5})\text{O}_3$  uncompensated weak ferromagnet, *J. Phys.: Condens. Matter* **21**, 486002 (2009).
- [42] W. Wernsdorfer, Classical and quantum magnetization reversal studied in nanometer-sized particles and clusters, *Adv. Chem. Phys.* **118**, 99 (2001).
- [43] W. T. Coffey, Y. P. Kalmykov, and S. V. Titov, *Thermal Fluctuations and Relaxation Processes in Nanomagnets* (World Scientific, Singapore, 2020).